Damage evolution analysis in a “spaghetti” bridge model using the acoustic emission technique

Article

Damage Evolution Analysis in a “Spaghetti” Bridge model using the Acoustic Emission Technique

Boris Nahuel Rojo Tanzi [1,‡], Mario Sobczyk [1,‡], Tiago Becker [1,‡], Luis Segovia [2,‡], Sabrina Vantadori [3,‡], Ignacio Iturrioz [1,‡], Giuseppe Lacidogna [4,‡*]

[1] Department of Mechanical Engineering, UFRGS, Porto Alegre, Brazil
[2] Department of Civil Engineering, UFRGS, Porto Alegre, Brazil
[3] Department of Engineering & Architecture, University of Parma, Parma, Italy
[4] Department of Structural, Geotechnical and Building Engineering, Politecnico di Torino, Turin, Italy
* Correspondence: giuseppe.lacidogna@polito.it
‡ These authors contributed equally to this work.

Abstract: This paper applies the Acoustic Emission (AE) Technique to analyze the damage process in a one-meter span bridge model built from spaghetti sticks during a loading test. The AE signals are analyzed in terms of four coefficients that are evaluated as predictors of structure failure, with frequency variation appearing as the strongest indicator of instability. The AE data are also compared to theoretical predictions given by the Bundle Model, confirming that underlying general patterns in damage processes are highly influenced by the geometric distribution of the structure and the loading pattern that is applied to it.

Keywords: Quasi-brittle Materials; Damage Process; Acoustic Emission.

Citation: Rojo Tanzi B. N., Sobczyk M., Becker T., Segovia L., Vantadori S., Iturrioz I., Lacidogna G. Damage Evolution Analysis in a “Spaghetti” Bridge model using the Acoustic Emission Technique. *Appl. Sci.* **2021**, *1*, 0. https://doi.org/

Received:
Accepted:
Published:

1. Introduction

Damage process in structures or materials undergoing unstable collapse is a widely studied topic because it occurs in many different situations, including catastrophic events with heavy human and economic tolls. This process is particularly important in the case of heterogeneous materials such as rocks, concrete ceramics, and other composites, either natural or artificial. According to [1], the main phenomena characterizing damage processes in these materials are: (i) significant size-effects in the strength and failure strain, (ii) transitions from uniform damage distribution to a clear discontinuity process, known as cracks localization, and (iii) the associative effect among clusters of micro-cracks, which can either intensify or inhibit damage propagation throughout the structure during the process.

Model parameters describing damage evolution can be represented by continuous regularization functions, which filter a series of discontinuities distributed throughout space and time, thus providing valuable information regarding the ongoing damage process, indicating how and when a significant loss of material resistance can occur. In its turn, collapse study by means of apparently simple theoretical models allows one to avoid the specifics of each structure and to perceive tendencies that are common to several systems, regardless of building materials, boundary conditions and problem scale. Some such models are discussed in [2]. Aided by these models, one can describe laws that apply to processes ranging from the rupture of biological materials of microscopic dimensions [3], to seismological events throughout hundreds of kilometers [4,5].

Besides pure Mechanics, similar patterns can be found in other realms of Physics, most notably the method of renormalization groups proposed by [6], which allows to cope with instability problems such as disruption of solids and phase changes. These ideas also apply to other instability problems, like those found in time series of economic indexes [7], the degradation of social systems [8], and the collapse of ancient civilizations

Nomenclature

ϵ	Exponencial coefficient of the cumulative number of events (N) vs. energy signal magnitude
A	Amplitude signal
$a(t)$	Amplitude of the record register by the divice during the time
A_p	Maximum Amplitude of the signal
A_{th}	Thresold
b	Exponencial coefficient of the cumulative number of events (N) vs. signal magnitudes (A)
c	Exponencial coefficient of the accumulated number of events (N) vs. characteristic signal frequency f_s
E_s	Signal Energy
f_s	Characteristic Signal frequency
N	Cumulative number of events
R_A	Rise Angle
R_T	Rise Time
t	Time
t_f	Final time
t_i	Initial time
t_p	Instant of the signal maximum amplitude
u	Displacement

[9]. In all these cases, studying the evolution of local instabilities throughout space and time is a fundamental step in predicting global instability.

In Mechanics, a suitable way to register local instabilities is the Acoustic Emission (AE) technique. Whether caused by a chemical reaction (metal corrosion), the spasmodic growth of vegetal, or an impact from an external source, among many other examples, when a local instability occurs, it is said to generate an event in a specific structure location, called *source*. This event causes the propagation of mechanical waves that are perceived by sensors on the structure's surface. By placing various sensors on suitable locations of the structure, space and time distribution of these events can be determined, and the parameters calculated from such measurements are a sensitive means for tracking changes within the studied structure.

Here, we apply the AE technique to track a small-scale bridge built from spaghetti sticks. As the bridge is subjected to increasing load, two sensors acquire the AE signals. Measurement results are compared to theoretical predictions according to the Bundle Model [10], which is widely used in this field [11]. This comparison's primary goal is to highlight the possibility of an underlying universal pattern for structures in collapse, which is often masked by specifics in geometry and boundary conditions imposed on each structure. The use of a spaghetti bridge as the basic structure for the study facilitates the execution of typical material tests – e.g., three-point bending and uniaxial compression in a cylinder – on an easy to build, inexpensive specimen. [12] have also explored this possibility, applying artificial intelligence methods to determine the collapse load on a similar bridge.

2. Theoretical Foundations

This work is based upon two basic tools: the Acoustic Emission technique, and the Bundle Model. The basic principles of each tool will be presented in this section.

2.1. Acoustic Emission Technique

When a mechanical system is excited by an external source or undergoes changes in its internal structure, it presents local instabilities (*events*) that propagate as mechanical waves. These Acoustic Emission (AE) signals are usually accelerations with frequencies ranging from 10^4 to 10^7 Hz [13]. These signals are detected by accelerometers mounted on the structure's surface, as depicted in Figure 1, where the excitation is usually a force or prescribed displacement in time.

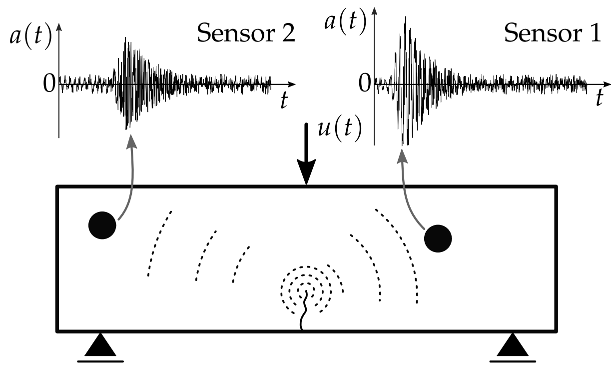

Figure 1. Basic setup for acquiring AE signals, with two AE sensors. Although both signals refer to the same event, they differ according to their positions along the structure.

67 A typical AE signal is illustrated in Figure 2. Several parameters can be extracted from these signals [13] but the ones of interest here are: maximum Amplitude (A_p), signal threshold (A_{th}), initial time (t_i), and final time (t_f), where both times are functions of the fixed threshold level. The Rise Time (R_T) is defined as $R_T = t_p - t_i$, i.e., the difference between the instant of maximum amplitude (t_p) and the moment t_i when amplitude rise from threshold levels was first detected. From these data, the Rise Angle (R_A) is given by $R_A = R_T/A_p$. Finally, the area under the signal is also of interest, because it bears a direct relation with the acoustic energy emitted during the event, as explained in detail in [14].

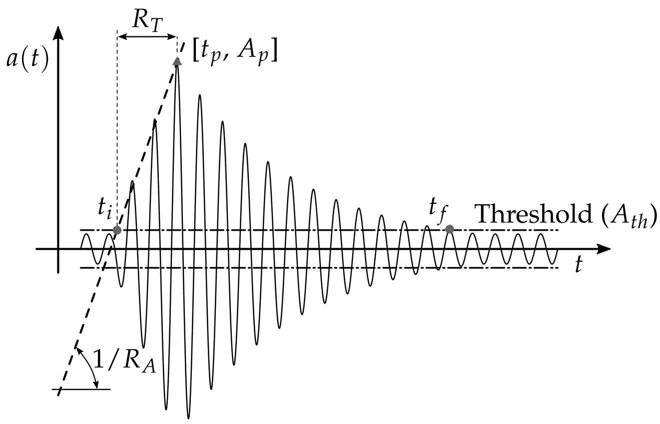

Figure 2. Typical AE signal with its parameters of interest.

76 Besides having their own meaning regarding both spatial and temporal distributions of the events in AE tests, these parameters can also be combined, generating reliable indicators regarding the possibility of system collapse. Such indicators are:

(a) **Relation between the number of events N and the signal amplitude A:** This relation has been long used in seismological applications, as illustrated by the classic Gutenberg & Ritcher law [4], which is of universal nature and does not depend on the scale of the distribution [11,15,16]:

$$N(\geq A) \propto A^{-b}, \tag{1}$$

79 where N is the cumulative number of signals and A is the signal amplitude. The physical meaning is discussed in [17–19]. It is hypothetically related, according to the expression $\mathcal{D} = 2b$, to the fractal dimension $\mathcal{D}$ of the material domain from which the signals generated by cracks are emitted. When the damage process begins within a structure, signals are emitted from a micro-cracks roughly evenly distributed in the material volume, i.e., $\mathcal{D} = 3$ and $b = 1.5$. Thus, according

to Eq. 1, most events produce small-amplitude signals. As damage advances, localization effects take place, and the signals are emitted preferentially from micro-cracks that distribute on preferential surfaces, which results in macro-crack nucleation. In this last phase, therefore, the values for $\mathcal{D}$ and b become 2 and 1, respectively, and the application of Eq. 1 yields an increase in the number of large-amplitude events. Thus, the evaluation of b and how it changes with time allows one to keep track of damage processes.
The procedure for computing b is described schematically in Figure 3a. The amplitudes due to each signals are collected and organized in a histogram. Then, a bi-log diagram is built to illustrate the cumulative number N of signals with amplitude $\geq A$. Finally, b is the angular coefficient of the fitting line. For a more detailed discussion about this computing procedure, see [20].

(b) **Relation between N and the signal energy emission E_s:** the energy carried in the signal is also related to N in a form similar to that of the amplitude A, using ϵ a fitting coefficient analogous to b:

$$N(\geq E_s) \propto {E_s}^{-\epsilon}. \tag{2}$$

The calculation of ϵ is analogous to the one described for b in case (a). It is also described in Figure 3b. Since the emitted AE signal energy is proportional to the squared maximum amplitude ($E_s \propto A^2$), it is apparent that the expected interval for b [1.0, 1.5] translates to [0.5, 0.75] for ϵ, as discussed in [2] and shown by numerical simulation in [21]. As Figure 3b also indicates, one can also compute the energy emission from the area under the signal envelope. This approach, referred to here as the RILEM method, was proposed in [13,22]. Finally, it is also possible to calculate energy emission from the Root Mean Square of the signal.

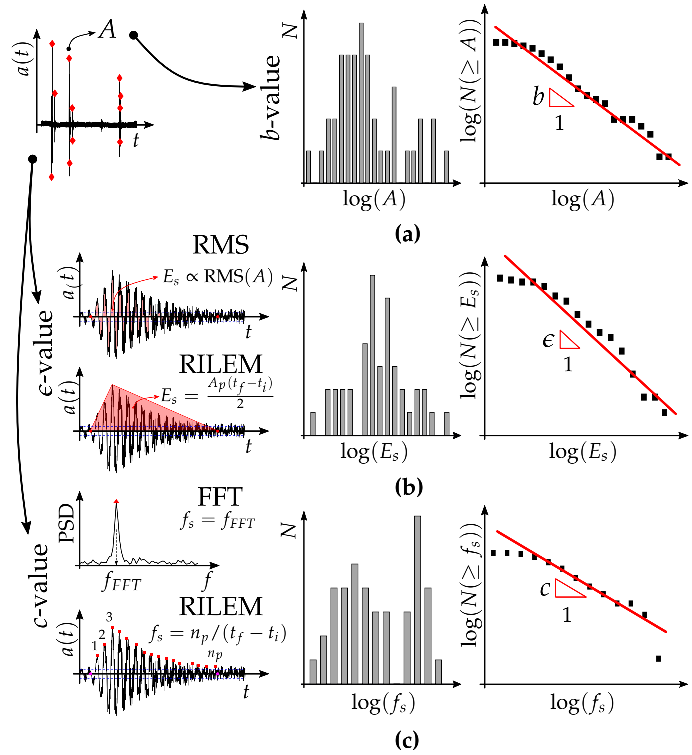

Figure 3. Precursors from AE tests, (a) obtaining b from Eq. 1; (b) calculation of ϵ from Eq. 2; (c) determining c from Eq. 3.

(c) **Relation between N and the characteristic signal frequency f_s:** this parameter was introduced by the same research team involved in this work as a reliable indicator for avalanches during a damage process [23]. This newly introduced coefficient c is also obtained by analogous means to those given for Eqs. 1 and 2, but focusing on the frequency distribution of the AE signals, i.e.:

$$N(\geq f_s) \propto {f_s}^{-c} \tag{3}$$

where N is the cumulative number of signals with frequencies greater or equal to f_s. The value of c can be calculated similarly to that used for b, as indicated in Figure 3c: it is the slope line of the signals distribution during the damage process as a function of the frequency that characterize the signals. As in the case of the b-value for amplitudes, the c-value indicates changes in the damage process and the imminence of collapse by keeping track of the acquired AE signals' frequencies. For instance, if the number of events with lower characteristic frequencies increases compared to the higher ones, a change in the damage process has occurred.

Still regarding Figure 3c, note that there are two ways to calculate the characteristic frequency f_s of the AE signal. The first is taking the ratio between the number of cycles np and the signal time interval $(t_f - t_i)$, as proposed by the [22] and referred to here as RILEM frequency. An alternative definition is by determining the spectral distribution of the AE signal and taking the frequency with the highest peak, i.e., the FFT method.

(d) **Frequency fluctuations during the damage process:** A well-known measure of energy fluctuations in AE signals relies on their dependence on signal frequency as described by the spectral density function (SDF), as mentioned by [24]. The first observations regarding this dependence are reported by [25], who coined the term $1/f$-noise or Flicker Noise when studying noise effects in electronic circuits. According to [26], the dependence of noise energy distribution with respect to frequency is given by:

$$E(f) = a\, 1/f^{\gamma}, \tag{4}$$

where $E(f)$ is the energy emission, f is the signal frequency, while γ and a are scalar fitting coefficients. Taking the logarithm of both sides in Eq. 4 the best fitting line leads to a linear law, where gamma is the angular coefficient. Its calculation is described schematically in Figure 4.

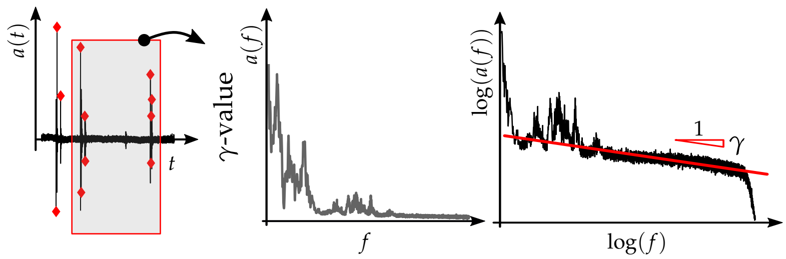

Figure 4. Relation between the power density spectrum and the frequency content, with calculation of the γ parameter.

As observed in [27] and many other works, this type of fluctuation is widely observed many different scientific fields, such as geology [28], finances (Kononovicius and Ruseckas, 2015), bioengineering [29], and even music [30,31]. Moreover, the distributions described in Eq. 4 is also observed to hold for frequencies ranging from fractions of hertz (in seismology) to gigahertz (microelectronics), which clearly illustrates the fractal character of this distribution and the phenomena to which it applies [27]. In the specific case of Acoustic Emission applications, the study of damage in historic buildings by [32] is an interesting example, where the exponent changes in the imminence of (either local or global) instabilities associated with structural collapse.

2.2. Bundle Model

The Bundle Model was proposed originally by [10] and exhaustively explored in [11]. Its simplest version is the *Equal Load Shared Bundle Model* (ELS Bundle Model), which comprises a set of parallel fibers (Figure 5a) with both ends fixed to a rigid frame. Each fiber is assumed to have elastic behavior until reaching its respective failure strength, which is given by a known statistical distribution. The typical load vs prescribed displacement for this setup is presented in Figure 5b. In the classical paper by [15], it is shown that when a continuously increasing displacement is prescribed to the set of fibers (i.e., the set is continuously stretched by infinitesimal increments), the distribution of number of broken bars is given by an exponential function with a universal exponent of -2.5, regardless of the specific distribution of failure strength in the fibers.

As shown in Figure 6, the ELS Bundle Model also predicts two forms of distributions that deviate from the aforementioned universal one. The first deviation takes place when the prescribed displacement is continuously increased only to a value $u_{xi} < u_{\max}$, i.e., the loading process is interrupted before the critical displacement for complete failure is reached. In this case, since the available data does not reflect the entire failure process, the model's predictions deviate from the universal distribution as shown in Figure 6a. The second form occurs when the prescribed displacement occurs in discrete steps. Now each step is large enough to cause failure of several fibers at once, causing the prediction curve to draw away from the ideal straight line at the top left of the graph, as shown in Figure 6b.

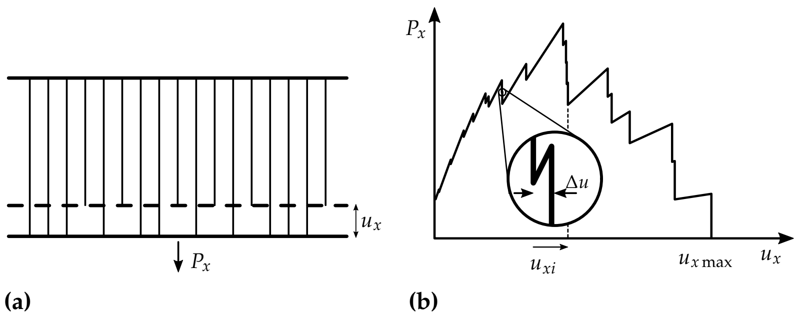

Figure 5. The Bundle Model. (a) Parallel bar model where a prescribed displacement u_x is applied and the reaction P_x is measured, (b) evolution of the load during the damage process in typical Bundle Model (Adapted from [11]).

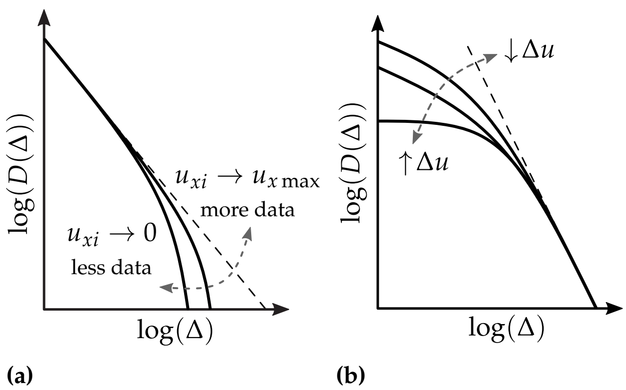

Figure 6. The avalanches distribution in the Bundle Model, defining avalanche as the number of bars that break simultaneously. (a) When the prescribed displacement is continuously increased, but the test is stopped before complete failure (i.e., $u_{xi} < u_{x\,\max}$). (b) When u_x is applied in discrete steps with amplitude δu.

3. Application: The Bridge Model Analysis

To illustrate the effectiveness of the global parameters' evolution obtained from an AE analysis method as predictors of structure collapse, the technique was applied to a small-scale bridge model made from spaghetti sticks. Such bridges are built to take part in a contest, which occurs twice a year at the Engineering School of Universidade Federal do Rio Grande do Sul (UFRGS), since 2004. Participation in the context is mandatory for Civil Engineering students, but it is also open to students from all other Engineering programs. The general guidelines for the contest (geometric restrictions, mass limits, load application, etc.) are given in [33], and the main geometric parameters are given in Figure 7.

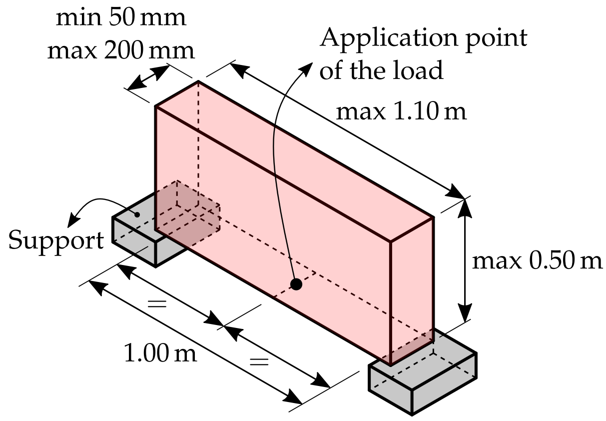

Figure 7. Geometric restrictions for the UFRGS Spaghetti Bridge contest (adapted from [33])

The collapse loads for all bridges evaluated in the contest are informed in Figure 8, with four winning designs being highlighted in the same figure and depicted in Figure 9. It is noticed that the average collapse load increases for the first six years, tending to an approximately constant value after that. This is due to the increased tendency of most contestants to adopt the topology depicted in Figure 9c, which is theoretically optimal for stiffness [34].

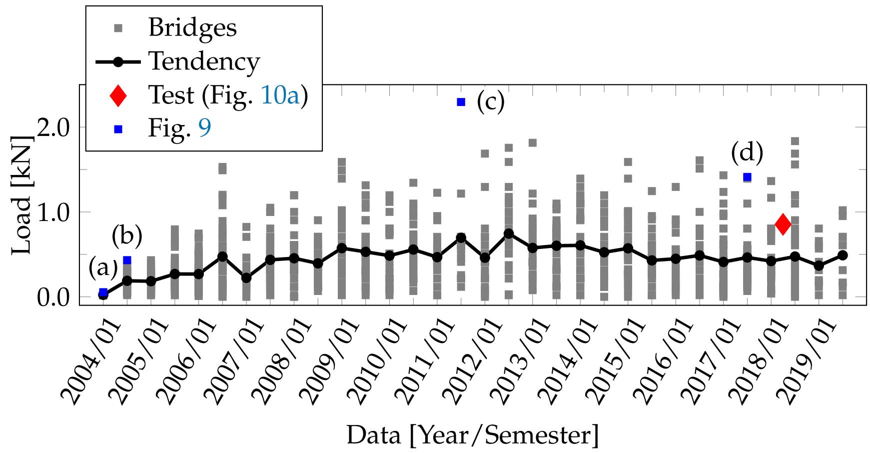

Figure 8. Evolution of collapse loads for the UFRGS Spaghetti Bridge contestants, data from [33].

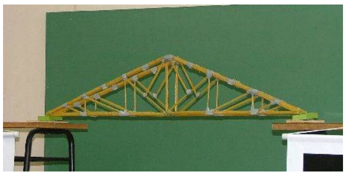

(a) 2004/01; 53.96 N.

(b) 2004/02; 431.64 N.

(c) 2011/02; 2295.54 N.

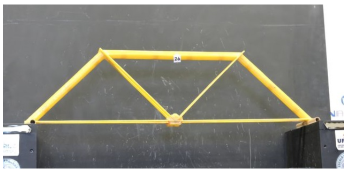

(d) 2017/02; 1412.62 N.

Figure 9. A few winning designs for the UFRGS Spaghetti Bridge contest, data from [33].

The spaghetti bridge used in the AE test is depicted in Figure 10, undergoing its load test during the contest, and its corresponding collapse load is also highlighted (in red) in Figure 8. This bridge was 1.08 m long, 0.15 m wide and 0.45 m high, with 1.40 kg of mass. Load was increasingly applied manually to its center line, with increments in 10 s intervals until collapse occurred at $t = 235$ s, with 784.80 N. Two accelerometers [35] were installed on the spots marked as S_1 and S_2 in Figure 10a, for acquiring the AE signals. These accelerometers are piezoelectric, with frequency measurement range from 5 kHz to 60 kHz. Their signal was acquired through a data acquisition module Brüel&Kjær® PULSE™ 3035, at a sampling rate of 65.54 kHz.

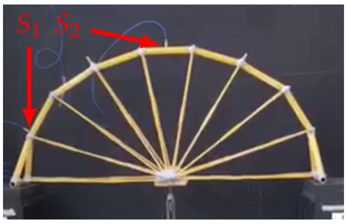

(a) 93.46 s.

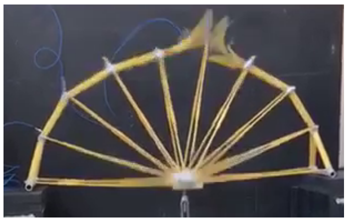

(b) 234.82 s.

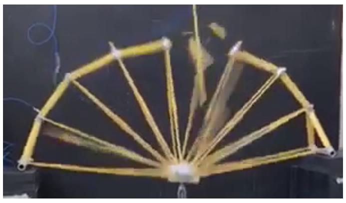

(c) 234.89 s.

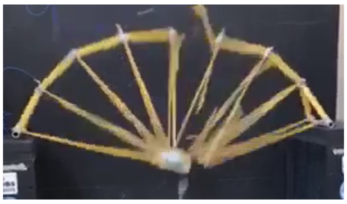

(d) 234.96 s.

Figure 10. Damage progress over time for the studied Spaghetti Bridge.

4. Results

Throughout the incremental loading test, 230 signals were detected by the AE sensors. The overall result is in Figure 11a, which also depicts a few typical signals for individual events. These results are also summarized in Figure 10b in terms of amplitude peak for each signal, and their cumulative number in relation to the load.

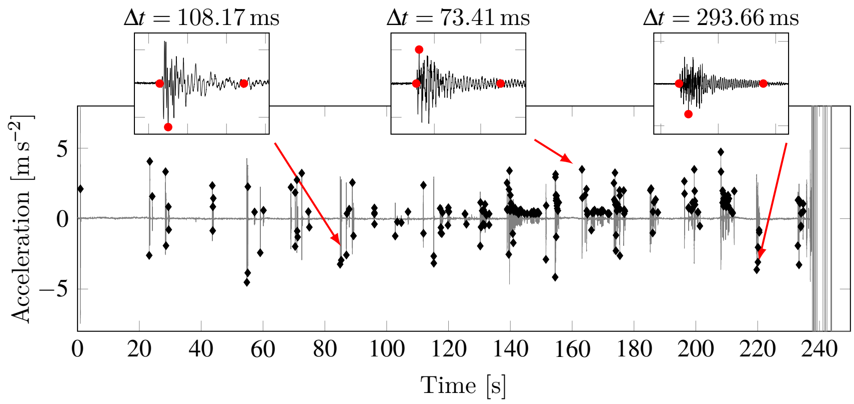

(a)

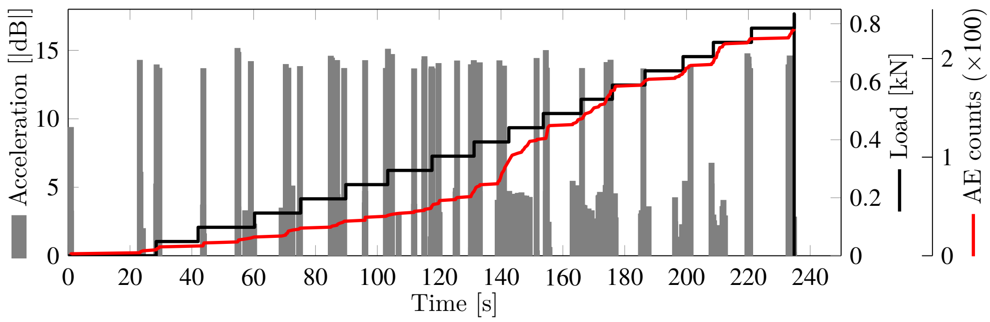

(b)

Figure 11. (a) AE data acquired during the loading test, with illustrating signals from individual signals. (b) Load applied to the bridge with corresponding signal counts.

Results show that signal occur nearly at the same time as the load is increased, indicating that signal distribution depends explicitly on the loading pattern. Also, for $t < 140\,\mathrm{s}$, the signal count grows at an approximately constant rate. When $t \cong 140\,\mathrm{s}$, there is a sharp increase in the number of signals. Finally, for $t > 140\,\mathrm{s}$, signal numbers grow once again at a nearly constant rate, but at a faster pace than that of the previous one.

4.1. *Evolution of coefficients b, ϵ, c*

The coefficients were calculated by separating the data set into packs of 25 events, with 5-event overlaps between successive packs. The coefficients evolution is presented in Figure 12, accompanied by the cumulative number of signals. The figure detail shows that the avalanche at $t \cong 140\,\mathrm{s}$ in Figure 11 matches sudden coefficient changes, especially b and ϵ, with higher variations of the latter when energy calculation uses RMS values. Moreover, the sharp variation in c occurs before the avalanche, which evidences this coefficient's usefulness as a precursor to the regime change.

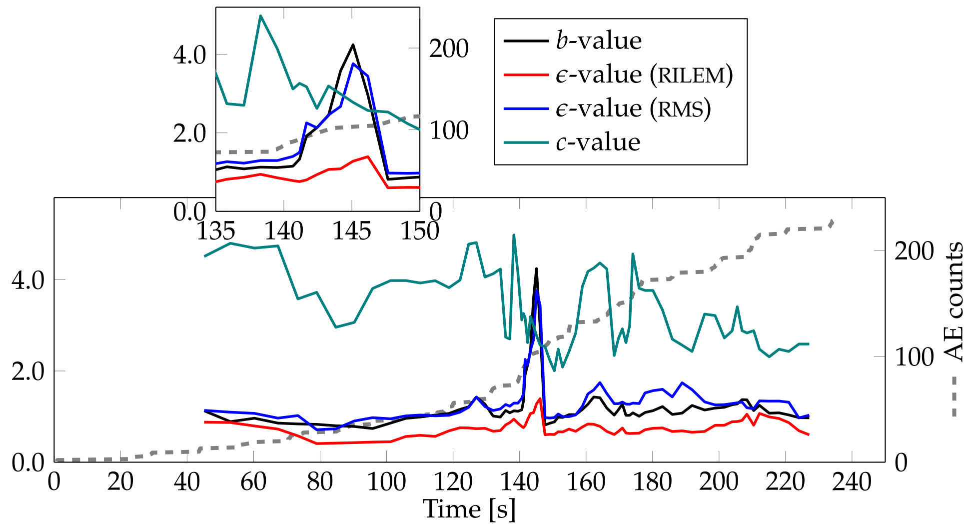

Figure 12. Time evolution of value-b, value-ϵ and value-c.

4.2. Frequency fluctuations during the damage process

The AE data set was divided into five intervals to evaluate frequency fluctuations, as shown in Figure 13. For each interval, the results from computing the Power Spectral Density were plotted in logarithmic scale, with a linear fit applied to the region where the frequency distribution approximates a straight line in the bi-log dominium, i.e., in the range from 10^3 to 10^4 Hz. The angular coefficient for the resulting fitting line is the parameter γ used to evaluate frequency fluctuation. Frequencies below 1 kHz cannot be reliably traced to the damage process because of interference with the structure's natural vibration modes. The marked attenuation for frequencies above 30 kHz is due to the anti-alias filtering embedded in the signals' electronic conditioning apparatus.

Still in Figure 13, the variation of γ is compared to load distribution and the cumulative number of events. The decrement of γ (and also of ϵ, already shown in Figure12) means that a wide band of frequencies is activated at each event, which agrees with the conclusions by [6] regarding unstable physical phenomena.

4.3. Comparison with the Bundle Model

Three histograms were computed to compare the AE-test results with the Bundle Model predictions: with the first 50% of observed signals, with the first 75% of signals, and with all signals. Corresponding results are depicted in Figure 14. This information is complemented by Figure 15, which illustrates a typical acceleration pattern observed throughout the tests. Due to measurement noise, a threshold $\log(0.2) = -0.7$ is used for computing the AE-signals. In Figure 14, this implies the nearly horizontal distribution obtained for small amplitudes: as small avalanches are undistinguished from measurement noise, the counting of AE-signals remains constant.

Comparing the results in Figure 14 to the theoretical predictions given by the Bundle Model in Figures 6a and 6b, it is possible to observe that:

1. Experimental results agree with the general shape predicted by the model, with a central part tending to a linear curve in the bi-log graph. This evidences that the damage process tends to occur according to an exponential function, but its characteristic exponent is different. The data are also consistent with the theoretically expected deviations towards both magnitude extremes.
2. Reducing the sample size for drawing the distribution does not affect AE-events distribution only at the magnitude extremes: when only the first 50% of the data are used, the intermediate linear range reduces in amplitude, and the angular coefficient is also affected.

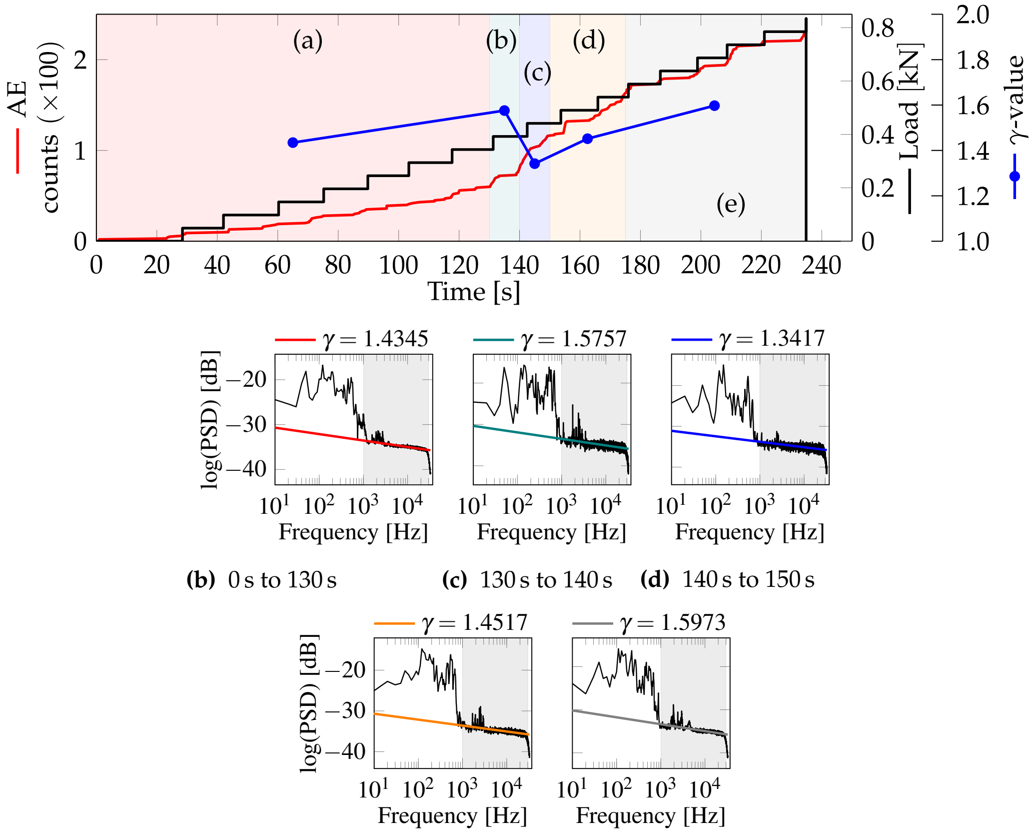

(b) 0 s to 130 s **(c)** 130 s to 140 s **(d)** 140 s to 150 s

(e) 150 s to 175 s **(f)** 175 s to 237.40 s

Figure 13. Evolution of γ throughout the AE test.

3. The results presented here suggest that the damage process occurs according to a general pattern similar to the one predicted by the Bundle Model. However, this tendency suffers in varying degrees from the effects of measurement noise, the structure's external geometry, the boundary conditions applied to it, and the internal organization of the system's elements. The influence exerted by these factors is illustrated schematically in Figure 16. The two extreme cases correspond to the predictions given by the Bundle Model when all fibers are aligned in parallel (a) or almost entirely in series (f), whereas cases (b)-(e) represent several combinations of geometry and externally applied loads, which appear as intermediate arrangements within the context of the model. Thus, the spaghetti bridge configuration studied here is closer to the quasi-serial Bundle Model (case (f)), which is more prone to localization effects than the other cases. Finally, due to the need to apply a threshold value for negating measurement noise effects, all profiles tend to a "platea" for small-amplitude events.

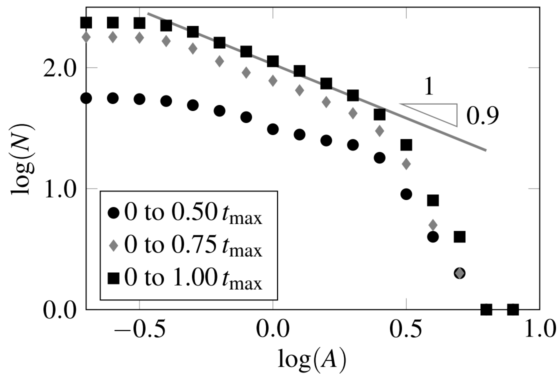

Figure 14. $N(A)$ –histograms from the AE– test results, taking into account, 50%, 75% and 100% of observed events.

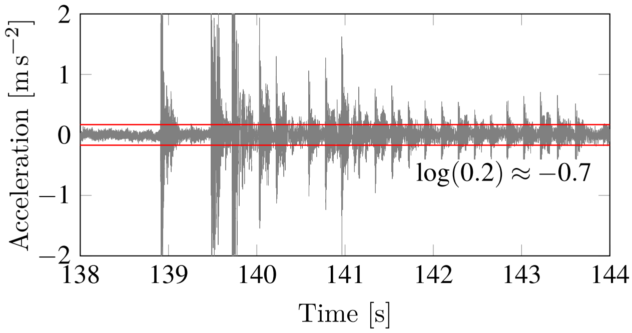

Figure 15. Acceleration pattern typically acquired during the tests, with the amplitude threshold that defined actual AE-signals.

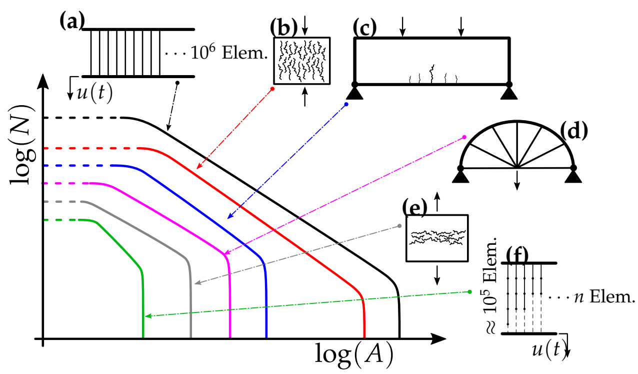

Figure 16. Frequency distribution of some measure of avalanches magnitudes in different structural typologies.

The following three examples reinforce the hypothesis presented in item (3):

(a) In seismology, [36] state that seismic events may result in any intermediate form between the extreme-case histograms illustrated in Figures. 17a and 17b, depending on several characteristics of the region where the event occurs.

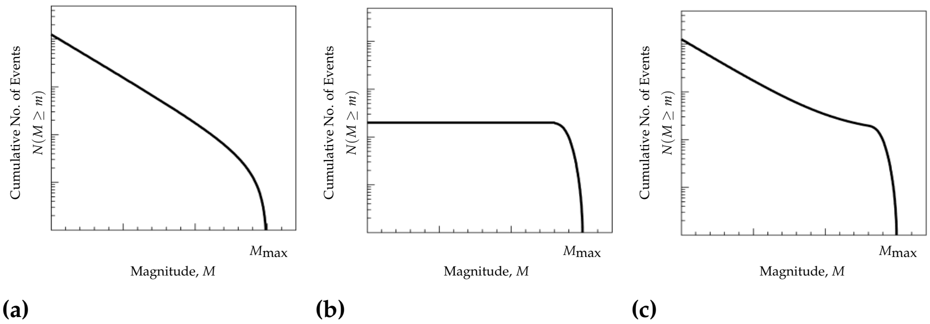

Figure 17. Histograms of earthquake temporal distribution, where $M = \log(A)$. (a) According to the universal law given by the Gutenberg-Richter model, which is similar to what is predicted by the Bundle Model. (b) Prediction for earthquakes with a definite magnitude. (c) Intermediate case. (From [36]).

(b) The behavior noted by [36] is also observed in the seismic behavior in the region of Angra dos Reis, Brazil, as evidenced by the corresponding histogram of seismic events in Figure 18.

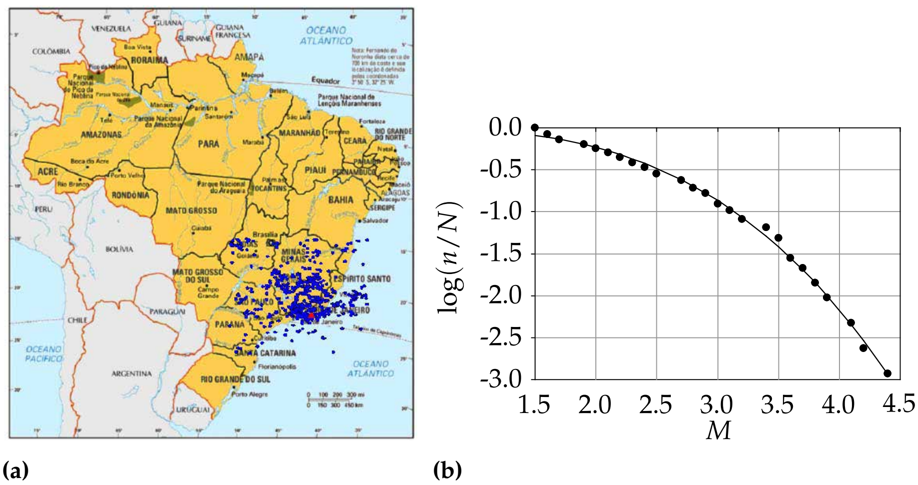

Figure 18. (a) Distribution of epicenters of seismic events with $M_w \geq 1.5$, recorded from 1959 to 2013 within a 1200 km^2 area in South-Eastern Brazilian SCR. The red point shows the site of the Angra dos Reis NPP (CNAAA). (b) Relation between $\log(n/N)$ for the region during the same period [37].

(c) In [37], a comparative analysis is made between a prismatic specimen under uniaxial compression and a pre-fissured beam under flexion on three points. Both structures were made from concrete, and the comparison was carried out both by numeric and experimental means. The results are summarized in Figure 19, making it clear that geometry and boundary conditions significantly influence structural behavior. For instance, the histogram for the beam tends to horizontal for small magnitudes because new ruptures tend to occur at the extremities of the pre-fissures, favoring localization of avalanches and connection between events. As for the prismatic specimen, ruptures are equally likely to appear at every part of its structure in the initial phases, with localization occurring only for advanced stages of the damage process.

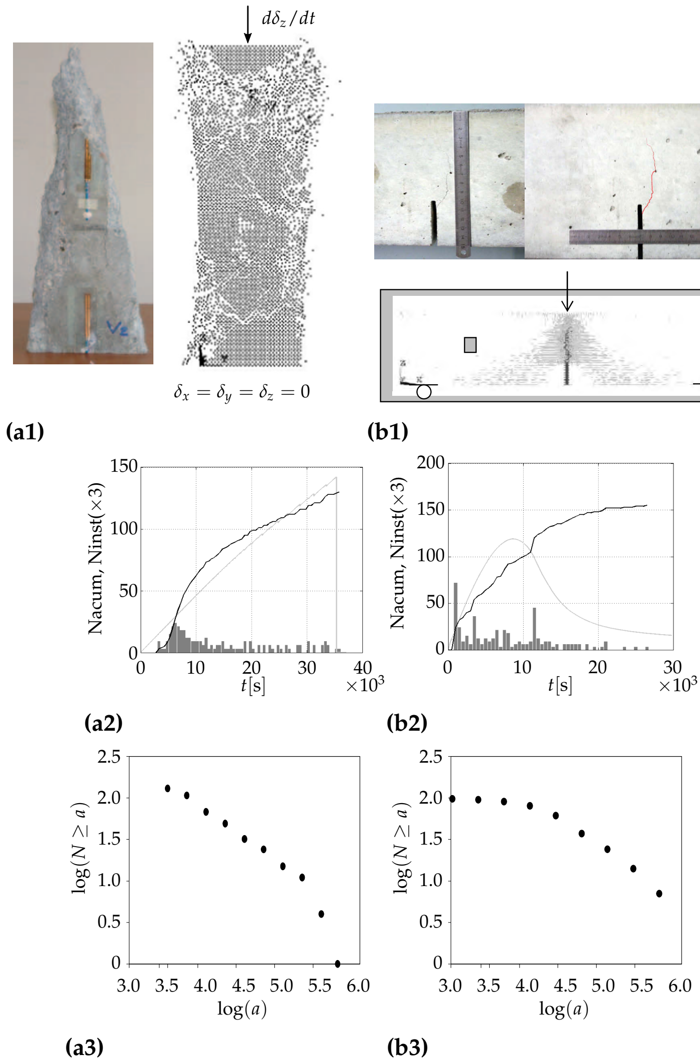

Figure 19. AE simulation results on concrete structures. (a) prism under uniaxial compression, (b) pre-fissured beam. (1) Results in terms of final configurations. (2) load vs time response (light-gray line), accumulated number of AE signals (dark line), and instantaneous distribution of events (histogram bars)(3) Accumulated number of signals vs their magnitudes in bilogarithmic scale [38].

5. Conclusions

In this work, acoustic emission (AE) data were collected from a load test applied to a small-scale spaghetti bridge model, where the load increased until the structure collapsed. Four different parameters (b, ϵ, c, and γ) were computed from the AE data, and their usefulness in identifying damage progression was evaluated. The main conclusions from such a procedure are:

- The evolution of the coefficients b, ϵ and c through time are suitable measures of the local instability associated with changes in the AE regime, with c (related with the event frequency distribution) being the most sensitive of the three.
- Computing ϵ from the RMS-value of the AE signal yields improved sensitivity compared to the traditional RILEM method.
- Analysis of frequency changes (variations in c and γ coefficients) are useful not only considering the isolated AE signals but also the complete information collected by the AE sensors. In particular, the γ coefficient presented a sharp reduction shortly before the localized damage became evident during the load test, which reinforces this coefficient's usefulness as a failure predictor.

- The minimum values for coefficients c and γ are consistent with the observations by [6] on the tendency of all phenomenon scales to participate when an instability occurs.
- Compared to the Bundle Model's theoretical predictions, experimental results presented here highlight the influence of boundary conditions, geometry, and internal organization on the collapse pattern of structures.

Acknowledgments: The authors would like to thank the CNPq (Brazilian National Council for Scientific and Technological Development) and FAPERGS (Foundation for Research Support of the State of Rio Grande do Sul of Brazil) for their financial aid in this work.

Conflicts of Interest: Declare conflicts of interest or state "The authors declare no conflict of interest." Authors must identify and declare any personal circumstances or interest that may be perceived as inappropriately influencing the representation or interpretation of reported research results. Any role of the funders in the design of the study; in the collection, analyses or interpretation of data; in the writing of the manuscript, or in the decision to publish the results must be declared in this section. If there is no role, please state "The funders had no role in the design of the study; in the collection, analyses, or interpretation of data; in the writing of the manuscript, or in the decision to publish the results".

Abbreviations

The following abbreviations are used in this manuscript:

AE	Acoustic Emission
CNAAA	Central Nuclear Almirante Álvaro Alberto
FFT	Fast *Fourier* Transform
UFRGS	Universidade Federal do Rio Grande do Sul
RILEM	International Union of Laboratories and Experts in Construction Materials, Systems and Struc
RMS	Root Mean Square

References

1. Krajcinovic, D. *Damage Mechanics*; Number 41 in North-Holland series in applied mathematic and mechanics, Elsevier: Amsterdam - New York, 1996.
2. Biswas, S.; Ray, P.; Chakrabarti, B.K. *Statistical Physics of Fracture, Breakdown, and Earthquake: Effects of Disorder and Heterogeneity*; John Wiley & Sons: Germany, 2015.
3. Gao, H. A Theory of Local Limiting Speed in Dynamic Fracture. *Journal of the Mechanics and Physics of Solids* **1996**, *44*, 1453 – 1474. doi:https://doi.org/10.1016/0022-5096(96)00038-5.
4. Richter, C.F. *Elementary Seismology*; Vol. 2, W. H. Freeman and Company and Bailey Bros. & Swinfen Ltd., 1958.
5. Turcotte, D.L.; Newman, W.I.; Shcherbakov, R. Micro and Macroscopic Models of Rock Fracture. *Geophysical Journal International* **2003**, *152*, 718–728. doi:10.1046/j.1365-246X.2003.01884.x.
6. Wilson, K.G. Problems in Physics with Many Scales of Length. *Scientific American* **1979**, *241*, 158–179. doi:10.1038/scientificamerican0879-158.
7. Rosser, J.B. The Rise and Fall of Catastrophe Theory Applications in Economics: Was the Baby Thrown Out with the Bathwater? *Journal of Economic Dynamics and Control* **2007**, *31*, 3255–3280. doi:10.1016/j.jedc.2006.09.013.
8. Hansen, H.F.; Hansen, A. A Monte Carlo Model for Networks Between Professionals and Society. *Physica A: Statistical Mechanics and its Applications* **2006**, *377*, 698–708. doi:10.1016/j.physa.2006.11.064.
9. Tainter, J.A. *The Collapse of Complex Societies*; New Studies in Archaeology, Cambridge Univ. Press: Cambridge, 1988.
10. Daniels, H.E. The Statistical Theory of the Strength of Bundles of Threads. I. *Proceedings of the Royal Society of London. Series A. Mathematical and Physical Sciences* **1945**, *183*, 405–435. doi:10.1098/rspa.1945.0011.
11. Hansen, A.; Hemmer, P.C.; Pradhan, S. *The Fiber Bundle Model: Modeling Failure in Materials*; Statistical Physics of Fracture and Breakdown, Wiley-VCH Verlag GmbH & Co. KGaA: Weinheim, 2015. OCLC: 905727775.
12. Riazi, A.; Karmo, D.; Ibrahim, M.A.S.; Amadou, S. Estimating the weight and the failure load of a spaghetti bridge: a deep learning approach. *Journal of Experimental & Theoretical Artificial Intelligence* **2020**, *32*, 875–884, [https://doi.org/10.1080/0952813X.2019.1694590]. doi:10.1080/0952813X.2019.1694590.
13. Grosse, C.; Ohtsu, M., Eds. *Acoustic Emission Testing*; Springer Berlin Heidelberg: Berlin, Heidelberg, 2008. doi:10.1007/978-3-540-69972-9.
14. Carpinteri, A.; Lacidogna, G.; Corrado, M.; Di Battista, E. Cracking and Crackling in Concrete-Like Materials: A Dynamic Energy Balance. *Engineering Fracture Mechanics* **2016**, *155*, 130–144. doi:10.1016/j.engfracmech.2016.01.013.

15. Hemmer, P.C.; Hansen, A. The Distribution of Simultaneous Fiber Failures in Fiber Bundles. *Journal of Applied Mechanics* **1992**, *59*, 909–914. doi:10.1115/1.2894060.
16. Shiotani, T.; Fujii, K.; Aoki, T.; Amou, K. Evaluation of Progressive Failure Using Ae Sources and Improved b-value on Slope Model Tests. Progress in Acoustic Emission Vii: Proceedings of the 12th International Acoustic Emission Symposium, Sapporo, Japan, October 17 - 20, 1994, International Acoustic Emission Symposium ; 12; Kishi, T., Ed.; , 1994; Vol. 7, pp. 529–534.
17. Aki, K. Scaling Law of Seismic Spectrum. *Journal of Geophysical Research* **1967**, *72*, 1217–1231. _eprint: https://agupubs.onlinelibrary.wiley.co doi:10.1029/JZ072i004p01217.
18. Carpinteri, A.; Lacidogna, G.; Puzzi, S. From Criticality to Final Collapse: Evolution of the "b-Value" from 1.5 to 1.0. *Chaos, Solitons & Fractals* **2009**, *41*, 843–853. doi:10.1016/j.chaos.2008.04.010.
19. Carpinteri, A.; Lacidogna, G.; Niccolini, G. Fractal Analysis of Damage Detected in Concrete Structural Elements Under Loading. *Chaos, Solitons & Fractals* **2009**, *42*, 2047–2056. doi:10.1016/j.chaos.2009.03.165.
20. Han, Q.; Wang, L.; Xu, J.; Carpinteri, A.; Lacidogna, G. A Robust Method to Estimate the b-Value of the Magnitude–Frequency Distribution of Earthquakes. *Chaos, Solitons & Fractals* **2015**, *81*, 103–110. doi:10.1016/j.chaos.2015.09.004.
21. Iturrioz, I.; Lacidogna, G.; Carpinteri, A. Acoustic Emission Detection in Concrete Specimens: Experimental Analysis and Lattice Model Simulations. *International Journal of Damage Mechanics* **2014**, *23*, 327–358. doi:10.1177/1056789513494232.
22. RILEM Technical Committee (Masayasu Ohtsu). Recommendation of RILEM TC 212-ACD: Acoustic Emission and Related NDE Techniques for Crack Detection and Damage Evaluation in Concrete*: Test Method for Classification of Active Cracks in Concrete Structures by Acoustic Emission. *Materials and Structures* **2010**, *43*, 1187–1189. doi:10.1617/s11527-010-9640-6.
23. Friedrich, L.; Colpo, A.; Maggi, A.; Becker, T.; Lacidogna, G.; Iturrioz, I. Damage process in glass fiber reinforced polymer specimens using acoustic emission technique with low frequency acquisition. *Composite Structures* **2021**, *256*, 113105. doi:10.1016/j.compstruct.2020.113105.
24. Kogan, S.M. Low-Frequency Current Noise with a 1/f Spectrum in Solids. *Soviet Physics Uspekhi* **1985**, *28*, 170–195. doi:10.1070/PU1985v028n02ABEH003853.
25. Johnson, J.B. The Schottky Effect in Low Frequency Circuits. *Physical Review* **1925**, *26*, 71–85. doi:10.1103/PhysRev.26.71.
26. Milotti, E. 1/f Noise: A Pedagogical Review. *Arxiv: Physics* **2002**.
27. Mandelbrot, B.B. *Fractals: Form, Chance, and Dimension*; Freeman: San Francisco, 1977. OCLC: 3154119.
28. Lovejoy, S.; Schertzer, D. Scaling and Multifractal Fields in the Solid Earth and Topography. *Nonlinear Processes in Geophysics* **2007**, *14*, 465–502. doi:10.5194/npg-14-465-2007.
29. Dave, S.; Brothers, T.; Swaab, T. 1/f Neural Noise and Electrophysiological Indices of Contextual Prediction in Aging. *Brain Research* **2018**, *1691*, 34–43. doi:10.1016/j.brainres.2018.04.007.
30. Pease, A.; Mahmoodi, K.; West, B.J. Complexity measures of music. *Chaos, Solitons & Fractals* **2018**, *108*, 82–86. doi:10.1016/j.chaos.2018.01.021.
31. Voss, R.F.; Clarke, J. 1/f Noise in Music and Speech. *Nature* **1975**, *258*, 317–318. doi:10.1038/258317a0.
32. Carpinteri, A.; Lacidogna, G.; Accornero, F. Fluctuations of 1/f Noise in Damaging Structures Analyzed by Acoustic Emission. *Applied Sciences* **2018**, *8*, 1685. doi:10.3390/app8091685.
33. Segovia González, L.A. Competição De Pontes De Espaguete, 2004.
34. DTU Mechanical Engineering.; DTU Compute. TopOpt, 2018.
35. PCB Piezotronics, I. PCB Piezotronics 352A60, 2008.
36. Bommer, J.; Stafford, P. Seismic Hazard And Earthquake Actions. In *Seismic Design of Buildings to Eurocode 8*, Ahmed Elghazouli ed.; CRC Press, 2016; pp. 7–40. doi:10.1201/9781315368221-3.
37. Riera, J.D.; Iturrioz, I. Considerations on the Diffuse Seismicity Assumption and Validity of the G-R Law in Stable Continental Regions (SCR). *Revista Sul-americana de Engenharia Estrutural* **2015**, *12*, 7–25. doi:10.5335/rsee.v12i2.4544.
38. Riera, J.D.; Iturrioz, I. Performance of the Gutenberg-Richter Law in Numerical and Laboratory Experiments; IASMiRT: San Francisco, California, USA, 2013.